Scanning capacitance characterization of potential screening in InAs nanowire devices

J. J. M. Law, S. A. Dayeh, D. Wang, and E. T. Yu[a)]
Department of Electrical and Computer Engineering, University of California, San Diego, La Jolla, California 92093-0407, USA

(Received 16 September 2008; accepted 14 November 2008; published online 7 January 2009)

We have used scanning capacitance microscopy and spectroscopy to examine the effects of micron-scale metal contacts, typically present in nanowire-based electronic devices, on carrier modulation and electrostatic behavior in InAs semiconductor nanowires. We observe a pronounced dependence of scanning capacitance images and spectra on distance between the scanning capacitance probe tip and nanowire contact up to distances of 3–4 μm. Based on the comparison of these data with results of finite-element electromagnetic simulations, we interpret these results as a consequence of electrostatic screening of the tip-nanowire potential difference by the large metal contact. These results provide direct experimental verification of contact screening effects on the electronic behavior of nanowire devices and are indicative of the importance of assessing and accounting for the effect of large-scale contact and circuit elements on the characteristics of nanoscale electronic devices generally. © *2009 American Institute of Physics*.
[DOI: 10.1063/1.3055367]

I. INTRODUCTION

Semiconductor nanowires offer promising capabilities for future high-performance electronic,[1] optoelectronic,[2] biomedical,[3] and thermoelectric[4,5] devices and platforms for basic investigations of electronic structure and carrier transport in low-dimensional systems. InAs nanowires, in particular, are a superb candidate for high speed, high density, and ultralow power circuits due to their narrow band gap (0.354 eV at 300 K),[6] high electron mobility—in excess of 33 000 $cm^2/V\,s$ in bulk material[7]—and surface Fermi-level pinning[8] in the conduction band, which allows for the formation of Ohmic contacts with relative ease. Because of the geometries often employed in nanowire-based devices, understanding the interaction and influence of nearby macroscale objects, such as bulk contacts on nanowire behavior, is of paramount importance. Conventional macroscopic electrical characterization techniques yield only limited and/or indirect understanding of the interactions and influences of macroscale and nanoscale objects, while scanning probe measurements of local electronic properties enable highly spatially accurate, nondestructive, and direct experimental characterization of these interactions.

We have used scanning capacitance microscopy (SCM) and scanning capacitance spectroscopy (SCS) in conjunction with finite-element numerical simulations to examine the effects of micron-scale metal contacts typically present in nanowire-based electronic devices on carrier modulation and electrostatic behavior in semiconductor nanowires. Our results reveal a remarkably strong dependence of the capacitance spectra on the distance separating the probe tip and the metal contact, extending to distances of 3–4 μm and beyond. This dependence is revealed by comparison of the SCM/SCS data with finite-element electrostatic simulations to be a consequence of electrostatic screening of the tip-nanowire potential difference by the large metal contact. These results provide direct experimental verifications of contact screening effects such as those postulated for carbon nanotube based devices.[9] The design and expected performance of nanowire-based electronic devices, most notably nanowire field-effect transistors, may be strongly influenced by these screening effects, and they are indicative of the importance of mitigating the effects of large-scale contacts and circuit elements on the performance of nanoscale electronic devices.

II. EXPERIMENT

Unintentionally doped *n*-type InAs semiconductor nanowires with diameters of 70–115 nm were grown by metal-organic chemical vapor deposition using colloidal Au nanoparticles as catalysts on thermally oxidized Si substrates. Details of the growth procedure and conditions have been described elsewhere.[10] Electrical device structures were fabricated by sonication of nanowires into an ethanol solution and deposition of the nanowires onto a thermally oxidized Si wafer, followed by 15 nm Ti and 85 nm Al metallization and Ohmic contact formation to single nanowires using electron-beam lithography and electron-beam evaporation of 2 μm wide metal strips.[11] Finally, a 73 nm Y_2O_3/ZrO_2 film, for which the relative dielectric constant is 12, was sputter deposited to act as the insulating layer between the probe tip and the nanowire surface. Top-gated current-voltage measurements of wires fabricated in this fashion were carried out to verify the Ohmic nature of the contacts and extract important device parameters such as mobility and carrier concentration. A Digital Instruments (Veeco) Nanoscope IIIa Dimension 3100 microscope with a diamond-coated probe tip was utilized to probe the nanowire capacitance versus voltage characteristics near a single contact, yielding both scan-

[a)]Electronic mail: ety@ece.ucsd.edu.

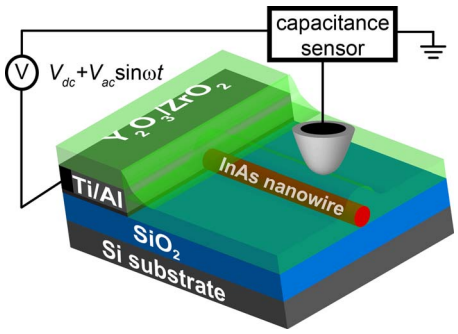

FIG. 1. (Color online) Schematic of sample structure, scanning probe measurement geometry, and voltage biasing arrangement.

ning capacitance images at fixed bias voltages and local spectra of the scanning capacitance signal dC/dV as a function of bias voltage. For SCM measurements, a bias voltage consisting of a dc component with a small (~2 V) ac modulation, typically at a frequency of 20–95 kHz, was applied to the sample with the probe tip grounded. For SCS measurements, the probe tip was held at a fixed position, while a low frequency (~0.5 Hz) saw-tooth wave of amplitude varying between 6 and 12 V and a high frequency (20–95 kHz) of ~2 V amplitude sine-wave bias were applied to the sample with the probe tip grounded. As discussed in detail elsewhere,[12–14] the SCM/SCS signal detection mechanism yields a voltage signal that is proportional in our measurements to dC/dV, where C is the tip-sample capacitance and V is the dc component of the applied bias voltage. Typical ambient conditions for these experiments were ~20 °C and ~50% relative humidity. For ease of interpretation in terms of analogous behavior of a conventional metal-insulator-semiconductor structure, for which it is typical to specify the voltage applied to the metal contact relative to the semiconductor, we at this point adopt the convention of specifying the potential of the probe tip V_{tip} relative to the sample in discussion and analysis of the SCM/SCS data. Figure 1 shows a schematic diagram of the sample and probe tip geometry employed in these experiments.

Finite-element electrostatic simulations were carried out using the commercial simulation package COMSOL MULTIPHYSICS. The simulation geometry sought to mimic the electrostatic environment in the experimental geometry as accurately as possible. Thus, a wire of 7 μm in length and 70 nm in diameter; a rectangular metallic contact of 7 μm in length (perpendicular to the axial direction of the nanowire), 3 μm in width (parallel to the axial direction of the nanowire), and 70 nm in height; and a probe with tip radius of curvature of 50 nm and of conical cross section of 7 μm in height and 3.5 μm in radius at the base were simulated. The wire and the contact were both conformally coated with a dielectric layer of 73 nm in thickness and with a relative dielectric constant $\varepsilon_r=12$. Further simulations were carried out with a smaller contact measuring 100 nm in length, 3 μm in width, and 70 nm in height in order reduce the cross-sectional area normal to the long axis of the wire. The wire was given the dielectric constant of bulk InAs ($\varepsilon_r=15$) (Ref. 7) and an electrical conductivity of 6×10^4 S/m, which is the value determined from current-voltage characteristics obtained

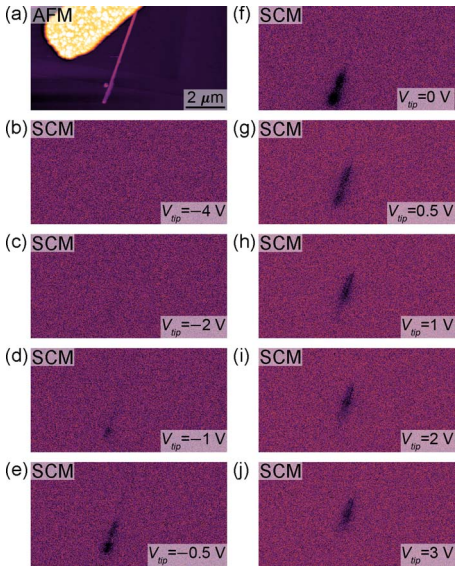

FIG. 2. (Color online) (a) AFM topograph with grayscale of 150 nm in height and [(b)–(j)] SCM images of an InAs nanowire and Al contact obtained at dc bias voltages of −4, −2, −1, −0.5, 0, 0.5, 1, 2, and 3 V, respectively.

from the wires in this experiment. Both the contact and the probe tip were treated as equipotential surfaces at varying static potentials with the contact permanently at ground while the tip was set at positive bias. The probe tip was placed at the apex of the wire/dielectric system and at regular intervals along the axial direction of the wire, as schematically illustrated in Fig. 1. The simulation yielded the potential profile of the entire simulated geometry.

III. RESULTS AND DISCUSSION

Figure 2(a) shows an atomic force microscopy (AFM) topograph of a nanowire and contact. Figures 2(b)–2(j) show the SCM images of the area corresponding to the topographic image in Fig. 2(a), obtained at dc bias voltages from −4 to +3 V and applied to the tip relative to the sample. Figures 2(b) and 2(c) show no SCM contrast, indicating that at these dc biases the dC/dV curve is flat, i.e., the wire is likely depleted or the capacitance change is no longer measurable by our instrument. With an increase in the dc bias to −1 V corresponding to Fig. 2(d), we begin to see a small amount of SCM contrast. At −0.5 and 0 V, shown in Figs. 2(e) and 2(f), the contrast level has increased dramatically. In Figs. 2(g)–2(i), the contrast begins to decrease but the center of the contrast area begins to move up toward the contact. More generally, as the dc voltage is increased from −4 to +3 V, the peak of the SCM signal contrast shifts closer to the metal contact. These results indicate that there is an additional influence on the device, for in a semiconductor nanowire (or planar device structure) of uniform doping and potential profile, $C(V)$ and thus dC/dV should be invariant as a function of position, resulting in a SCM image of the nanowire that shows constant signal contrast across the entirety of the sample.

Figure 3(a) shows an AFM topograph of another InAs nanowire, in this case nearly perpendicular to the contact. The wire is approximately 6.5 μm in length and slightly

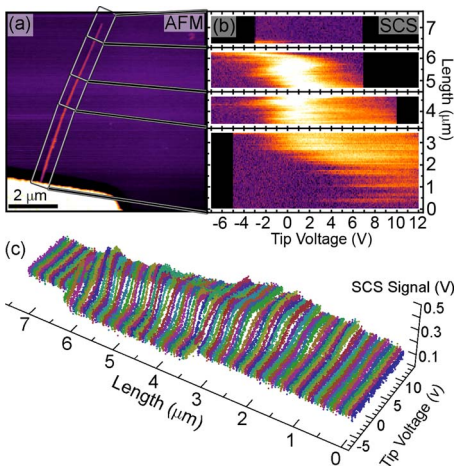

FIG. 3. (Color online) (a) AFM topograph with grayscale of 150 nm in height, (b) density plot of SCM signal vs length along the nanowire, and (c) individual line slices of SCM data as a function of tip voltage and length along the nanowire. Black regions in (b) indicate that data are not collected.

tapered. Figure 3(b) shows a density plot of the scanning capacitance spectra versus distance along the wire. Figure 3(b) consists of four separate plots, for which the data were collected, from top to bottom in the following dc tip voltage ranges: −3–7 V, −7–7 V, −7–10 V, and −5–12 V. The topographic region that corresponds to each of these sections is marked by boxes in Fig. 3(a). Some portions of the top- and bottom-most density plots correspond to areas where there is no wire, as seen in the corresponding boxed regions of Fig. 3(a). The black portions of Fig. 3(b) indicate voltage ranges where no data were collected. It is evident from the density plot that the dC/dV versus V behavior of the wire is not uniform along the length of the wire. Near the contact, the peak of the SCS signal decreases in value and shifts toward higher voltages as the tip approaches the contact. There also appears to be a slight broadening of the peak in the dC/dV versus V curves near the contact. Several microns away from the contact, the SCM signal contrast is larger and varies little as a function of distance from the contact.

Figure 3(c) shows a three-dimensional plot of the scanning capacitance signal as a function of tip voltage and distance from the contact in 100 nm increments. From this figure, it is evident that the peak of the dC/dV versus V spectra shifts to larger positive voltages as the tip approaches the contact. Qualitatively, this behavior is similar to that seen in Fig. 2, leading us to conclude that the angle between the wire and the contact has a relatively little influence on the qualitative behavior of the system. Each of the dC/dV spectra was fitted using a polynomial and subsequently differentiated to find the voltage at which the peak in the dC/dV occurs as a function of tip-contact distance. This voltage is plotted as a function of the tip distance from the contact in Fig. 4(a). Spectra taken less than one micron away from the contact had peaks at voltages larger than the 12 V limit of our instrument, as shown in Fig. 3(c); thus they are not included in Fig. 4(a). Some of the spectra near the noncontacted end of the nanowire had peaks that were too small to definitively extract a peak; thus these values were also not included. We attribute the negative voltage of the peaks occurring at approximately 6 μm in Fig. 4(a) to the presence of localized charge between the wire surface and the oxide, which would cause a shift in the associated dC/dV spectra. However, the overall trend of the curve remains the same. Figure 4(a) explicitly demonstrates that the maxima in the dC/dV spectra, and correspondingly the threshold voltage for electron accumulation at the InAs surface, shift substantially, and in a highly nonlinear fashion, as a function of distance from the contact.

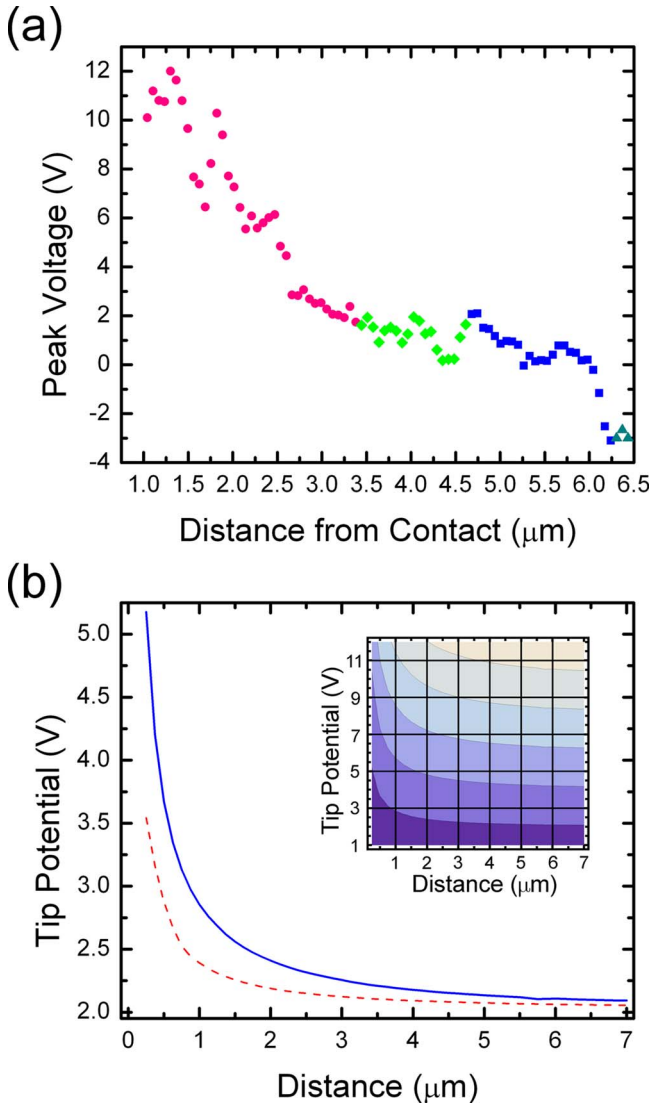

FIG. 4. (Color online) (a) Plot of the voltage of the peak of the dC/dV curve vs the tip distance from the contact with different shapes corresponding to the different sections in Figs. 3(a) and 3(b). (b) Plot of tip voltage required to produce constant potential (2 V) at the nanowire surface directly below the tip for a 7 μm long contact (solid line) and a 100 nm long contact (dashed line) showing the reduced effects of the screening for the smaller contact geometry. (Inset) Plot of constant surface potential contours directly beneath the tip for a 7 μm long contact vs tip voltage and the separation between the tip and the contact.

Examination of the tip-sample capacitance behavior as a function of distance between the probe tip and a nearby large-area contact reveals the strong influence of the large contact on the local electrostatic behavior of the nanowire. Local nanoscale carrier modulation characteristics and electrostatic behavior of the nanowire vary substantially as a

function of distance from the nanowire/contact interface. Specifically, the threshold voltage for carrier accumulation at the InAs surface shifts to lower voltages as the distance from the contact increases, indicating that the large contact screens a significant portion of the electric field from the scanning probe tip even at distances from the contact as large as a few micrometers. A highly nonlinear dependence of the screened potential on contact-tip spacing is observed. We note that the threshold voltage of our devices occurs at positive voltages despite negative threshold voltages in the literature for similar devices;[15] we speculate that this may be due to a combination of surface or interface charges, the small electron affinity of diamond and, thus, the correspondingly large surface potential difference between our tip and the InAs nanowire. Finally, in our experimental geometry, the metal contact is 100 nm tall in the direction perpendicular to the substrate and the nanowire's diameter is 70 nm, also perpendicular to the substrate, and as a result, the sputter-coated oxide near the contact-nanowire interface has a shape that is a superposition of both the contact and the nanowire; thus, the increased thickness of the oxide near the contact changes the amount of screening by the large contact and complicates the electrostatic behavior of the nanowire very close to the contact.

Figure 4(b) shows the results of finite-element electromagnetic simulations of the tip-sample experimental geometry. For each point in the upper left inset of Fig. 4(b), a separate simulation was carried out. Each simulation placed the tip at a different distance from the contact. The contact potential was kept at 0 V and the tip was held at potentials varying between 1 and 12 V in increments of 1 V. Each simulation generated the potential profile for the entire structure, and the inset in Fig. 4(b) shows a plot of the constant potential contours for potentials directly beneath the tip at the interface between the nanowire and the oxide for each of the simulated tip-contact distances and tip potentials. Figure 4(b) shows one such line of constant nanowire surface potential; in this case, the surface potential is 2 V and the applied tip voltage required to reach this potential value at the nanowire surface is plotted versus the distance. The potential seen on the wire surface can deviate substantially from the potential applied to the tip, as is evident in the inset of Fig. 4(b). This effect is especially noticeable as the tip nears the contact. For distances less than 1 μm, the screening effect is such that the potential at the wire surface can be reduced by 60% or more compared to the tip potential. This situation is somewhat analogous to drain induced barrier lowering seen in planar, short-channeled metal-oxide-semiconductor field-effect transistors.[16] Figure 4(b) demonstrates that in order to maintain a constant surface potential, i.e., as is required to operate a field-effect transistor in any bias range (e.g., accumulation, depletion, or inversion), it is necessary to apply an exponentially increasing amount of voltage to the gate as the gate-source separation is decreased. Nominally, there should be a voltage drop across the oxide which will never allow the potential at the wire-oxide interface to reach the potential on the metal gate; the dependence of this voltage drop on tip-contact distances, as shown in Fig. 4(b), demonstrates that a dramatic electrostatic screening effect is present, and that there is a highly nonlinear increase in the amount of electrostatic screening as the probe tip is moved closer to the large metallic contact.

In order to achieve a given surface potential for the nanowire, one must apply a voltage to the tip that varies strongly with the distance separating the contact and the tip. In an idealized case of no screening, the voltage drop across the oxide would be constant regardless of the distance between the tip and the contact. These results demonstrate directly that the geometry of the contacts has a dramatic influence on screening of nanoscale gate contacts in a geometry similar to that of a nanowire field-effect transistor. A reduction not necessarily in contact volume but in the cross-sectional area of the contact facing the nanowire should reduce the amount of coupling that the large contact has on the device. The effect of changing the source geometry is demonstrated in simulations of devices with smaller contacts. Replacing the 7 μm$\times$3 μm$\times$70 nm contact in our simulations with a contact that is 100 nm$\times$3 μm$\times$70 nm dramatically reduces the screening effect, as demonstrated by the dashed line in Fig. 4(b).

Charge transfer due to the difference in work function between the metal contact and the semiconductor nanowire can also result in an inhomogeneous potential profile along the nanowire,[9] which could be an alternate explanation for the trend seen in the data. This effect would persist regardless of the contact geometry and/or the presence of a scanning probe tip and is dependent only on the work function difference between the metal and the semiconductor. Thus, the variation in the effect with contact geometry, as evidenced in the simulations, and the SCS curve broadening near the contact suggest that the effect is more likely a result of contact potential screening. Other experimental results in the literature suggest that screening can be significantly reduced with a change in the gate and/or source/drain geometry, as shown recently in studies revealing a reduction in the parasitic effects of source/drain field coupling to the nanowire by making nickel silicide source and drain contacts to group IV core-shell nanowires.[17] These effects are expected to have substantial implications for the design and performance of nanowire-based electronic devices, most notably nanowire field-effect transistors. More generally, these results are indicative of the importance of assessing and accounting for the effect of large-scale contact and circuit elements on the characteristics of nanoscale electronic devices.

IV. CONCLUSIONS

In summary, we have used AFM, SCM, SCS, and finite-element electrostatic simulations to characterize and analyze the effects of micron-sized contacts to InAs nanowire devices in producing strong electrostatic potential screening that can have severe deleterious effects on nanowire device performance. A screening effect was directly observed and found to shift the threshold voltage of the devices by several volts over distances of several microns. The screening effect was established to be present on multiple nanowires with differing contact geometries. This effect should not be limited to InAs and should persist in any semiconductor material

system. Through simulation, these observations were shown to be a direct result of the relative size of the nanowire compared to the contact and the shape of the probe-tip gate. A simulated reduction in the cross-sectional area of the contact helped suppress the screening effect, consistent with the behavior seen in recently reported experiments. These results have implications for the design and performance of a variety of nanowire-based electronic devices. Moreover, the results highlight the importance of understanding and accounting for the electrostatic interaction between nano- and macrosized objects in nanoscale devices.

ACKNOWLEDGMENTS

We would like to acknowledge the financial support from the Office of Naval Research (ONR-nanoelectronics) and the National Science Foundation (Grant No. ECS-0506902).

[1]Z. Zhong, D. Wang, Y. Cui, M. W. Bockrath, and C. M. Lieber, Science **302**, 1377 (2003).
[2]M. H. Huang, S. Mao, H. Feick, H. Yan, Y. Wu, H. Kind, E. Weber, R. Russo, and P. Yang, Science **292**, 1897 (2001).
[3]O. Ambacher, J. Majewski, C. Miskys, A. Link, M. Hermann, M. Eickhoff, M. Stutzmann, F. Bernardini, V. Fiorentini, V. Tilak, B. Schaff, and L. F. Eastman, J. Phys.: Condens. Matter **14**, 3399 (2002).
[4]A. I. Boukai, Y. Bunimovich, J. Tahir-Kheli, J. Yu, W. A. Goddard III, and J. R. Heath, Nature (London) **451**, 168 (2008).
[5]A. I. Hochbaum, R. Chen, R. D. Delgado, W. Liang, E. C. Garnett, M. Najarian, A. Majumdar, and P. Yang, Nature (London) **451**, 163 (2008).
[6]Z. M. Fang, K. Y. Ma, D. H. Jaw, R. M. Cohen, and G. B. Stringfellow, J. Appl. Phys. **67**, 7034 (1990).
[7]S. M. Sze and K. K. Ng, *Physics of Semiconductor Devices*, 3rd ed. (Wiley, New York, 2007), p. 789.
[8]C. A. Mead and W. G. Spitzer, Phys. Rev. Lett. **10**, 471 (1963).
[9]J. Guo, J. Wang, E. Polizzi, S. Datta, and M. Lundstrom, IEEE Trans. Nanotechnol. **2**, 329 (2003).
[10]S. A. Dayeh, E. T. Yu, and D. Wang, J. Phys. Chem. C **111**, 13331 (2007).
[11]S. A. Dayeh, D. P. R. Aplin, X. Zhou, P. K. L. Yu, E. T. Yu, and D. Wang, Small **3**, 326 (2007).
[12]C. C. Williams, J. Slinkman, W. P. Hough, and H. K. Wickramasinghe, Appl. Phys. Lett. **55**, 1662 (1989).
[13]Y. Huang and C. C. Williams, J. Vac. Sci. Technol. B **12**, 369 (1994).
[14]D. M. Schaadt, E. J. Miller, E. T. Yu, and J. M. Redwing, J. Vac. Sci. Technol. B **19**, 1671 (2001).
[15]S. A. Dayeh, C. Soci, P. K. L. Yu, E. T. Yu, and D. Wang, Appl. Phys. Lett. **90**, 162112 (2007).
[16]S. M. Sze and K. K. Ng, *Physics of Semiconductor Devices*, 3rd ed. (Wiley, New York, 2007), p. 333.
[17]Y. Hu, J. Xiang, G. Liang, H. Yan, and C. M. Lieber, Nano Lett. **8**, 925 (2008).